Title
Observing ion diffusion and reciprocating hopping motion in water

Journal
Science Advances, 9(30)

ISSN
2375-2548

Authors
Liu, Sangui
Han, Xinbao
Ophus, Colin
et al.

Publication Date
2023-07-28

DOI
10.1126/sciadv.adf8436

CHEMISTRY

Observing ion diffusion and reciprocating hopping motion in water

Sangui Liu[1]†, Xinbao Han[1,2]†, Colin Ophus[3], Shiyuan Zhou[1], You-Hong Jiang[1], Yue Sun[1], Tiqing Zhao[1], Fei Yang[4], Meng Gu[4], Yuan-Zhi Tan[1], Shi-Gang Sun[1], Haimei Zheng[5,6]*, Hong-Gang Liao[1]*

When an ionic crystal dissolves in solvent, the positive and negative ions associated with solvent molecules release from the crystal. However, the existing form, interaction, and dynamics of ions in real solution are poorly understood because of the substantial experimental challenge. We observed the diffusion and aggregation of polyoxometalate (POM) ions in water by using liquid phase transmission electron microscopy. Real-time observation reveals an unexpected local reciprocating hopping motion of the ions in water, which may be caused by the short-range polymerized bridge of water molecules. We find that ion oligomers, existing as highly active clusters, undergo frequent splitting, aggregation, and rearrangement in dilute solution. The formation and dissociation of ion oligomers indicate a weak counterion-mediated interaction. Furthermore, POM ions with tetrahedral geometry show directional interaction compared with spherical ions, which presents structure-dependent dynamics.

INTRODUCTION

Direct observation of ions in solution is crucial for understanding the existing form, interaction, and dynamics of ions, which is also essential to fundamental chemistry and applications (*1*, *2*). It is generally accepted that ion pairing, describing the association of two oppositely charged simple ions in solution, can be classified into solvent-separated, solvent-shared, and direct contact type (*3*, *4*). In past decades, many researchers studied different ions in solution by using variety of analytical techniques including small-angle x-ray scattering, static and dynamic light scattering, ultraviolet-visible spectroscopy, nuclear magnetic resonance spectroscopy, dielectric relaxation spectroscopy, atomic force microscopy, and confocal microscopy to understand the elementary processes (*2*, *5*–*8*). However, these conventional measurements based on the data averaged over time and/or species number are difficult to explore because of the ion dynamics at the molecular scale. Colloidal solution containing charged particles decorated with ligands and their counterions, as a mimic system of real solution, enables researchers to probe dynamics of imitation ions on a single-unit scale with microscopy and to study the kinetics of nucleation and crystallization (*9*–*11*). Recently, the developments of liquid phase transmission electron microscopy (LPTEM) and cryo-TEM provide an opportunity to visualize the dynamics of nanomaterials or molecules in much smaller length and time scale (*12*, *13*). Particularly, in situ LPTEM have been used to elucidate nucleation and growth process of metals, oxides, semiconductors, and biomolecules (*14*–*19*). Very recently, Clark *et al*. (*20*) measured platinum adatom motion at solid-liquid interfaces using a graphene liquid cell in a TEM. However, direct observation of the existing form, interaction, and dynamics of real ions or molecules in solution has not been achieved so far.

Polyoxometalates (POMs) are a class of soluble ionic metal oxide clusters principally constituted by tungsten, molybdenum, vanadium, niobium, and tantalum, which feature well-defined and unique structural motifs (*21*–*23*). These features make POM ion serve as a valuable model system for understanding of single ion dynamics and interionic interaction in solution (*21*, *24*). On the other hand, the inclusion of many electron-rich transition metal atoms provides excellent contrast in water during imaging. Recently, POM molecules have been used as a monomer model to study the assembly and nucleation by cryo-TEM (*25*, *26*). However, cryo-TEM characterization necessitated a vitrified solution, in which the motion of POMs was suppressed. Besides, additional counterions and their co-ions were involved in these observations. More authentic dynamics of ions in real solution with high spatial-temporal resolution is particularly appealing, whereas direct imaging individual ions in liquid is challenging because of the high phase contrast of liquid layer.

To visualize the dynamics of individual ions in solution, we developed a nanogap liquid cell, allowing ultrathin liquid film (around 50 nm) to be sandwiched between two 10-nm-thick Si_3N_4 membranes (figs. S1 and S2). This nanogap liquid cell inside for our LPTEM experiments enables a single-ion level imaging under low electron dose rate. Here, we present the structural detail of a single POM anion. Using the POM solution as a model system, we successfully captured the real-time motion of isolated ions and their interaction dynamics. An unexpected local reciprocating ion hopping occurs besides Brownian motion. We then observed the existence and structure evolution of ion oligomers and conducted quantitative analyses based on millisecond temporal resolution imaging.

[1]State Key Laboratory of Physical Chemistry of Solid Surfaces, Collaborative Innovation Center of Chemistry for Energy Materials, College of Chemistry and Chemical Engineering, Xiamen University, Xiamen 361005, China. [2]College of Chemistry and Chemical Engineering, Lanzhou University, Lanzhou 730000, China. [3]National Center for Electron Microscopy, Molecular Foundry, Lawrence Berkeley National Laboratory, Berkeley, CA 94720, USA. [4]Department of Materials Science and Engineering, Southern University of Science and Technology, Shenzhen 518055, China. [5]Materials Science Division, Lawrence Berkeley National Laboratory, Berkeley, CA 94720, USA. [6]Department of Materials Science and Engineering, University of California, Berkeley, CA 94720, USA.
*Corresponding author. Email: hmzheng@lbl.gov (H.Z.); hgliao@xmu.edu.cn (H.-G. L.)
†These authors contributed equally to this work.

RESULTS AND DISCUSSION

Diffusion dynamics of ions show local reciprocating hopping motion

A dilute aqueous solution of polyoxomolybdate $\{(NH_4)_{42}[Mo^{VI}_{72}Mo^{V}_{60}O_{372}(CH_3COO)_{30}(H_2O)_{72}]\cdot ca.300H_2O\cdot ca.10CH_3COONH_4$ (MoPOM)}, a well-studied Keplerate-type spherical POM anion $[Mo^{VI}_{72}Mo^{V}_{60}O_{372}(CH_3COO)_{30}(H_2O)_{72}]^{42-}$ (fig. S3), was prepared and injected into a nanogap liquid cell. The liquid cell was then sealed and loaded into TEM. The sealed ultrathin solution was imaged by spherical aberration coefficient (Cs)–corrected TEM. Figure 1A shows high-resolution (HR) images of individual MoPOM ions from different orientations; spherical hollow structure with a diameter of around 2.9 nm was observed. As confirmed by the simulated images (Fig. 1, B and C, and fig. S3D), MoPOM ions registered along different viewing directions show distinguishable detailed structures.

To monitor diffusion and interaction of individual ions, we imaged the ions at a lower magnification with a low electron beam dose rate of around 80 e $Å^{-2}$ s^{-1} (movie S1). TEM snapshots (Fig. 2, A and D, and fig. S3B) show that individual MoPOM ions can be clearly identified. Dynamics of single ion were tracked and quantified. During this period of movement, an unexpected local hoping motion occurs (Fig. 2, B and C, and fig. S4). The distinct movement, characterized by a burst of displacement (3 to 6 nm) and returning to previous position less than 1 s, is similar to the ion hopping in solid polymer electrolytes (*3*, *27*, *28*). In addition, in the observations of other two individual MoPOM ions (Fig. 2, D to F, and fig. S5), another three-position loop motion of ion hopping takes place (Fig. 2F, middle panel, and fig. S5B).

To quantify this distinct motion of ions in solution, we estimated the two-dimensional diffusion coefficient (*D*) (see figs. S6 and S7). The diffusion of POM ions is different from that of Au nanoparticles. In polymer electrolytes, ions can hop along polymer chain, between different polymer chains, or from polymer chain to free medium and vice versa (*27*, *28*). In highly concentrated liquid electrolytes, ion hopping motions takes place in the aggregated structure involving ions, co-ions, and solvents (*29*). The aggregate provides closely placed bridging coordination sites that could promote ion hopping. In our case of dilute solution in ultrathin liquid cell, water molecules may polymerize locally via hydrogen bonding with participation of counterion NH_4^+ (*30*, *31*) and behave like a molecular bridge in short range (Fig. 2G). Single ion can hop back and forth repeatedly through the short-range molecular bridge. The bridging zone allows fast ion hopping motion, whereas slow ion diffusion takes place once the ion is released into bulk solution medium. The hopping motion is barely affected by changing electron beam dose rate, which indicates that electrostatic interaction between the POM ions and Si_3N_4 surface did not affect the hoping motion (figs. S8 and S9). Furthermore, our experiments show that changing ionic strength of the POM ion solution by addition of NaCl affect the frequency as well as step length of hopping motion (fig. S10). These results support that molecular bridge is responsible for the hopping motion.

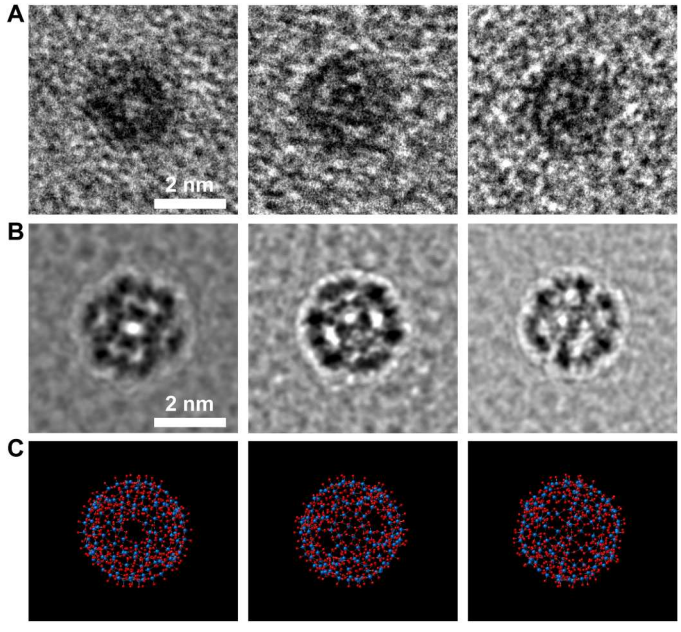

Fig. 1. Structure of MoPOM ions in water. (**A**) Cs-corrected high-resolution transmission electron microscopy (HRTEM) images with different orientation. (**B**) Corresponding simulated TEM images. (**C**) Ball-and-stick illustrations of corresponding crystallographic structures.

Counterion-mediated attraction between POM ions

When isolated MoPOM ions in free motion occasionally encounter each other in close distance, pairwise interaction can take place and lead to formations of dimer and trimer (movies S2 to S6). In dilute solution, the pairwise interaction and consequent oligomers formation widely exist (figs. S3B and S11). The oligomers, especially dimers, undergo frequent reversible combination and separation. Statistics of dimerization events (fig. S12) show that single ion and dimer exhibit similar dynamic behavior, which might arise from the weak interaction between ions (*21*).

To analyze ions interaction quantitatively, we tracked the evolution of surface distance between two pairwise ions in 153 s (Fig. 3, A and B, and movie S6). Two MoPOM ions dimerize and separate several times. Distance of dimerizing and separating events suggests that pairwise process is quite reversible (Fig. 3, C and D). Furthermore, the average velocity of one ion approaching another is plotted as a function of distance (Fig. 3E). The result shows that ions move randomly when interion spacing is beyond a critical distance of around 5 nm. Statistic of six dimer formations shows an average distance of 5.3 nm before the ion accelerated and moved together (fig. S13A). Because the interions are spacing down to 5 nm, the ion acquires a velocity increasing, with the distance decreasing and the velocity reaches the maximum speed at 2.3 nm surface distance, and then decreases as two ions get closer. This behavior indicates a complex attractive force between ions in short range, which is different from nanoparticles (*32*, *33*). The interaction force (right-hand axis of Fig. 3E) responsible for velocity was calculated by assuming the fluctuation dissipation theorem holds and using the following equation

$$F = k_B T v / D \quad (1)$$

Where *D* is the measured two-dimensional diffusion coefficient (fig. S6). v, k_B, and *T* are the obtained velocity, Boltzmann constant, and temperature (kelvin), respectively. Thus, the calculated forces between two pairwise ions are about 70 and 378 pN at distance of 4.0 and 2.3 nm, respectively. At the same distance, the attractive van der Waals (vdW) forces are calculated to be 0.14 and 0.8 pN,

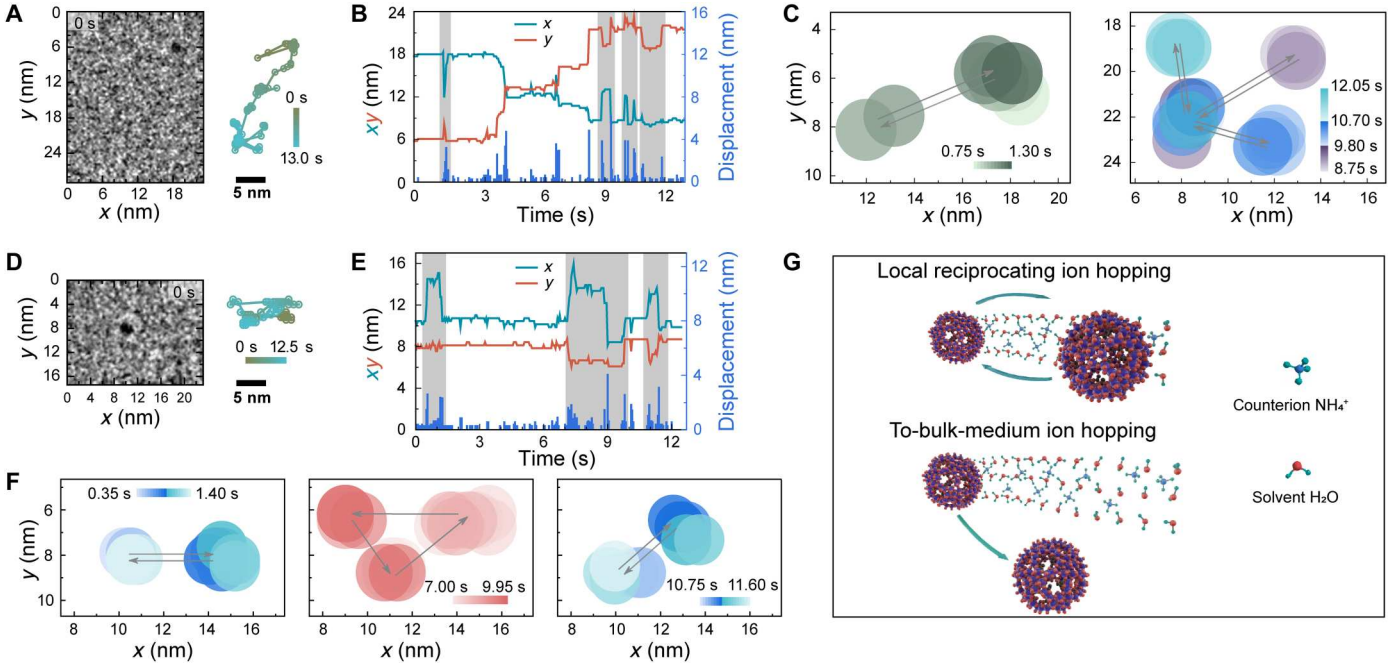

Fig. 2. Diffusion dynamics of single ions showing local reciprocating ion hopping motion. (**A** to **C**) Single ion I. (**D** to **F**) Single ion II. (A) and (D) TEM image of two individual ions and corresponding trajectory (movie S1). (B) and (E) Position and instantaneous displacement. Distinct movements are highlighted in gray-shaded regions. (C) and (F) Sketches illlustrate these ion local reciprocating hopping motion details. Round spot symbolizes the single ion, and color gradient refers to elapsed time of a hopping event. Arrow indicates the hoping direction. (**G**) Proposed mechanism of local reciprocating ion hopping through short-range polymerized bridge of solvents molecules and counterions or to-bulk-medium diffusion.

respectively. The measured force is three orders of magnitude larger than vdW force, which implies that there is additional force other than vdW force to dominate the pairwise interaction.

Pairwise interaction between two same charge MoPOM ions in solution is complicated, usually involving the counterions. Simulations (*34*, *35*) and experimental evidences (*36*, *37*) have proved that counterions could stay near the POM ion by associating or condensing to form a layer. On the basis of the quantitative analyses, we conclude that the MoPOM ion interaction is dominated by counterion-mediated attraction. As described in the scenario (Fig. 3B), MoPOM anions with associated counter-cation layer keep separate at a distance of around 5 nm, at which long-range electrostatic repulsion and vdW attraction are delicately balanced (*38*, *39*). For two MoPOM ions that overcome the repulsion because of thermal fluctuations, the distance gets close to about 4.0 nm, their respective counterion layers begin to fuse, and counterions are accumulated in between two MoPOM ions. Thus, counterion-mediated attraction dominates the interaction and results in two MoPOM ions rapidly approaching. This sharp increase in force (Fig. 3E) can be attributed to the depletion effect of accumulated counterions as the distance decreases (*34*). Notably, the force decreases after the distance reaching 2.3 nm, which is approximately one counterion layer thickness of 2.0 nm (*36*, *37*). In this distance, a strong association between counterions with both two MoPOM anions has arisen, thus making the removal of the shared counterions difficult because of an extra barrier. However, counterion-mediated attraction still drives the pairwise process, and two ions eventually form a dimer with the redistribution of counterions. The maximum distribution of interions spacing of dimers is around 0.2 nm (fig. S13B), indicating that counterion NH_4^+ or solvent H_2O barely stay in between the two MoPOM anions. It coincides with the evidence that counterions and/or solvent molecules distribute as a crown around the POM dimer "straits" and barely stay in the interion region, where the counterion crown facilitates stabilizing the oligomer (*40*–*42*).

Structure-dependent oligomer formation

We also investigated formation dynamics of oligomeric trimer (movies S7 and S8), tetramer (movie S9), and pentamer (movie S10). Figure 4A shows that the oligomer grows by single ion attachment, wherein the additional ion can be both an existing single ion and an isolated one dissociated from another oligomer. During attachment process, the additional ion attaches direct to the existing oligomer, and assembling angle changes slightly before the formation of new oligomer (Fig. 4B). The result indicates a random nondirectional interaction of oligomer formation for MoPOM.

We further probed the dynamics of another POM ion (figs. S14 and S15), $[\{Co_4(OH)_3PO_4\}_4(SiW_9O_{34})_4]^{32-}$ (CoPOM) with a tetrahedral structure and four concave faces (*43*). Structure-dependent formation and evolution of ion oligomer was revealed. Figure 5 (A to C) shows a pattern rearrangement of a trimer. During the observation (movie S11), one ion in the trimer (the left pale dark spot in Fig. 5A) moves vigorously, resulting in the trimer transforming its pattern between an obtuse triangle (60.7 s) and linear shape (113.6 s). Eventually, the trimer forms a stable pattern of approximate equilateral triangle (panel at 243.9 s in Fig. 5, A and C). Figure 5 (D to F) shows the formation of a tetramer by attachment of single ion to a preexisting trimer with triangular pattern (see movie S12).

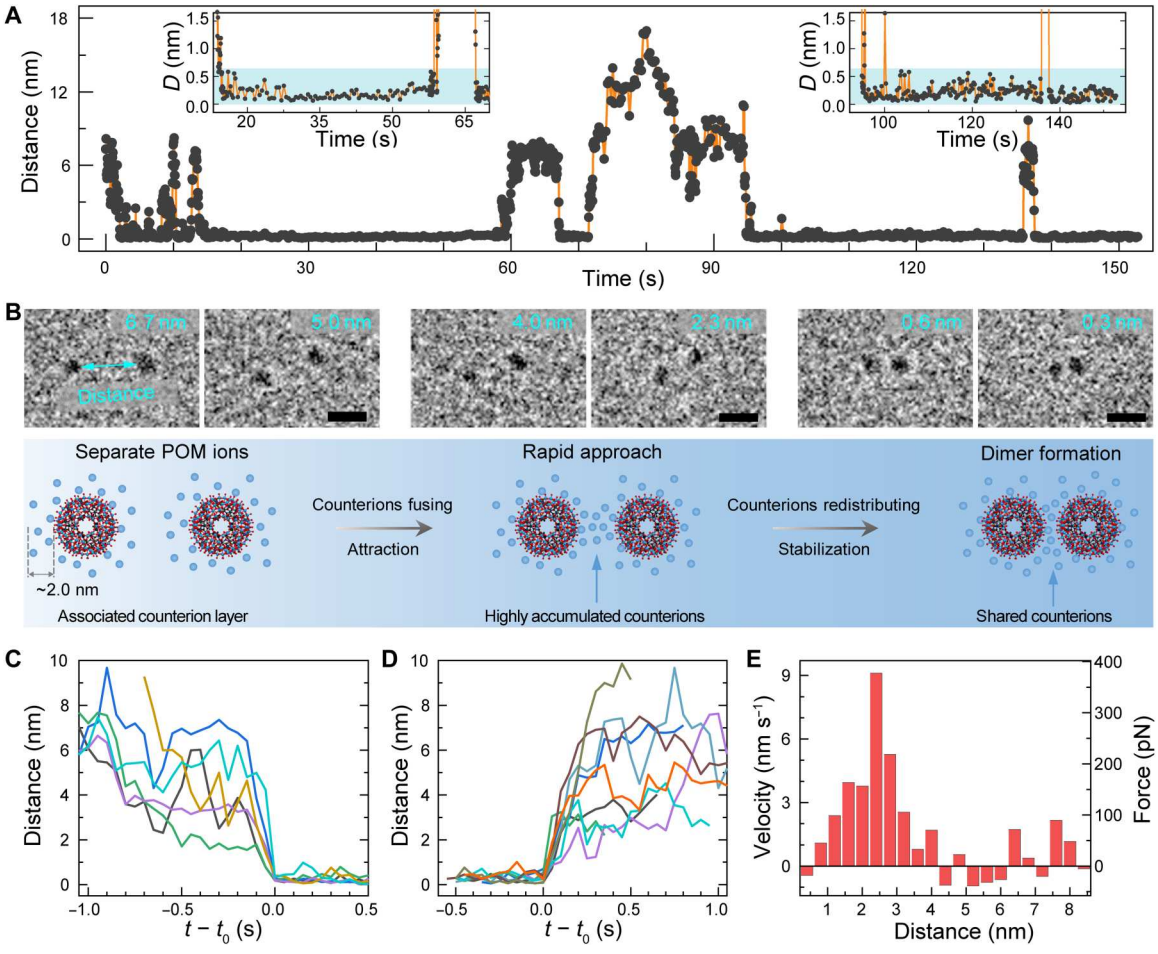

Fig. 3. Interaction dynamics between two pairwise ions. (**A**) Surface-to-surface distance evolution between two ions illustrating reversible formation and separation of a dimer. The insets show the formation of dimer (distance is smaller than 0.7 nm). (**B**) TEM images with distance label showing the three typical stages and corresponding sketch illustrating dynamics of counterion-mediated attraction. Scale bars, 5 nm. POMS, polyoxometalates. (**C** and **D**) Distance as a function of time during the dimer formation and separation, which shows the reversible pairwise interaction ($t - t_0 = 0$ s). (**E**) Velocity and interaction force as a function of distance.

By tracking the trajectory of the additional ion, we found that during the approaching, the ion first moved toward one side of the trimer and attached to the existing patterned trimer, forming a triangular-patterned tetramer (Fig. 5D). After that, the tetramer transforms into a quadrangular pattern (26.5 s) through site shifting of the additional ion (Fig. 5E), which shows a similar rearrangement behavior to that of the trimer in Fig. 5B. The evident direction changing from around 120° to 60° (Fig. 5F) is different from MoPOM, indicating a direction specific interaction between additional ion and preexisting trimer.

Such behavior of CoPOM ions differing from that of MoPOM ions may be related to their molecular structures and consequent distributions of counterions. For spherical MoPOM ion, homogenous distribution of counterions around POM ion leads to random nondirectional interaction during oligomer formation, without experiencing transitional pattern rearrangement. However, for tetrahedral CoPOM ion with four concave faces, its counterions prefer condensing at the concave face (fig. S14), resulting in the directional assembly driven by counterion-mediated attraction. This is supported by theoretical simulations that Keggin-type POM $\{SiW_9M_3\}$ ion shows inhomogeneous distribution of molecular electrostatic potentials (*44*) and the consequent preferred location of its associated counterions (*38*, *45*).

Oligomer dynamic structural transformation

Despite of the difference of interaction dynamics during the formation, oligomers for both ions exhibit dynamic structure change later (movies S13 to S16). According to our observation, oligomer can be described as four typical configurations, triangular, quadrangular, linear, and separated pattern (Fig. 6A and fig. S16). Pattern evolutions of four oligomers (two for CoPOM ions and two for MoPOM ions) show that oligomers can transform their configurations among four patterns (Fig. 6B and figs. S17 to S20). To evaluate the stability of the oligomer roughly, time duration of four patterns is analyzed (Fig. 6C and fig. S21). The result shows that the triangular pattern exists for the longest time, which can be attributed to many configurational isomers (fig. S22). Considering this fact, quadrangular pattern is the most stable configuration for tetramer MoPOM. For spherical MoPOM ions, 13 transformation events occurred within 3.35 s and experience highly dynamic structural transformation, and its oligomer can transform configuration between any two of four patterns (Fig. 6, B and E). However, the

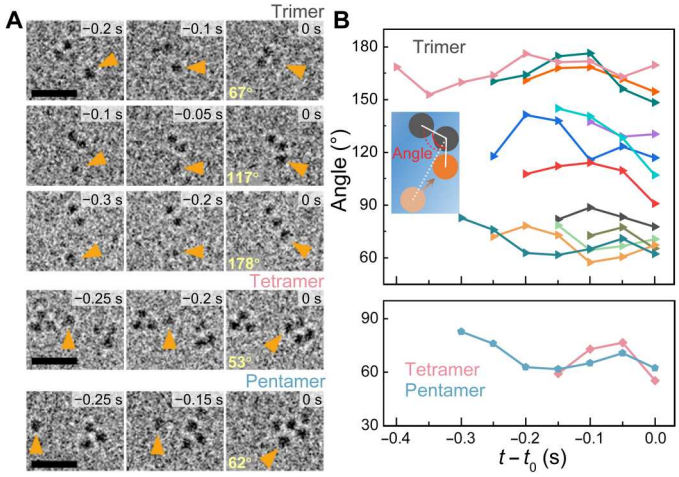

Fig. 4. Random attach formation of MoPOM ion oligomers. (**A**) TEM images showing three representative assembly processes of trimer (assembling angle is 67°, 117°, and 174°, respectively), tetramer (53°), and pentamer (62°). The additional ion is marked by orange arrow. Scale bars, 10 nm. (**B**) Angle evolution during last 0.4 s before the assembling at $t - t_0 = 0$ s. The statistics show no obvious assembling angles change, suggesting a nondirectional assembly. The inset illustrates assembling angle defined by additional ion (orange sphere) and existing oligomer (gray spheres). Arrow indicates the movement of the attaching ion.

transformation from linear or separated pattern to quadrangular pattern was not observed for CoPOM oligomer (Fig. 6, B and D). These absent actions indicate the existence of a barrier hindering free pattern transformation, which might arise from the tetrahedral geometry of CoPOM ion and corresponding distribution of counterions. These observations suggest that configurations of the oligomers in solution are highly transformable. We could conclude that oligomers remain in a transformable metastable state that undergoes rearrangement, separation, and recombination.

To summarize, our LPTEM study reveals an unexpected local ion hopping motion of POM ions in water. POM ions in dilute solution readily form oligomers, which is driven by a counterion-mediated interaction. The oligomers undergo frequent configuration transformation and exhibit structural dependent behavior. Our real-time observation of ions diffusion and interaction dynamics provides fundamental understanding of ions in solution.

MATERIALS AND METHODS

Synthesis of POMs

MoPOM was synthesized according to Müller's procedure (*46*). Briefly, first, $(NH_4)_6Mo_7O_{24}{\cdot}4H_2O$ (5.6 g, 4.5 mmol) and CH_3COONH_4 (12.5 g, 162.2 mmol) was dissolved in 250 ml of water in a 500-ml flask, and $N_2H_4{\cdot}H_2SO_4$ (0.8 g, 6.1 mmol) was then added. After stirred for 10 min, the solution was mixed with 83 ml of 50% CH_3COOH (aq). The mixture was stored in the open

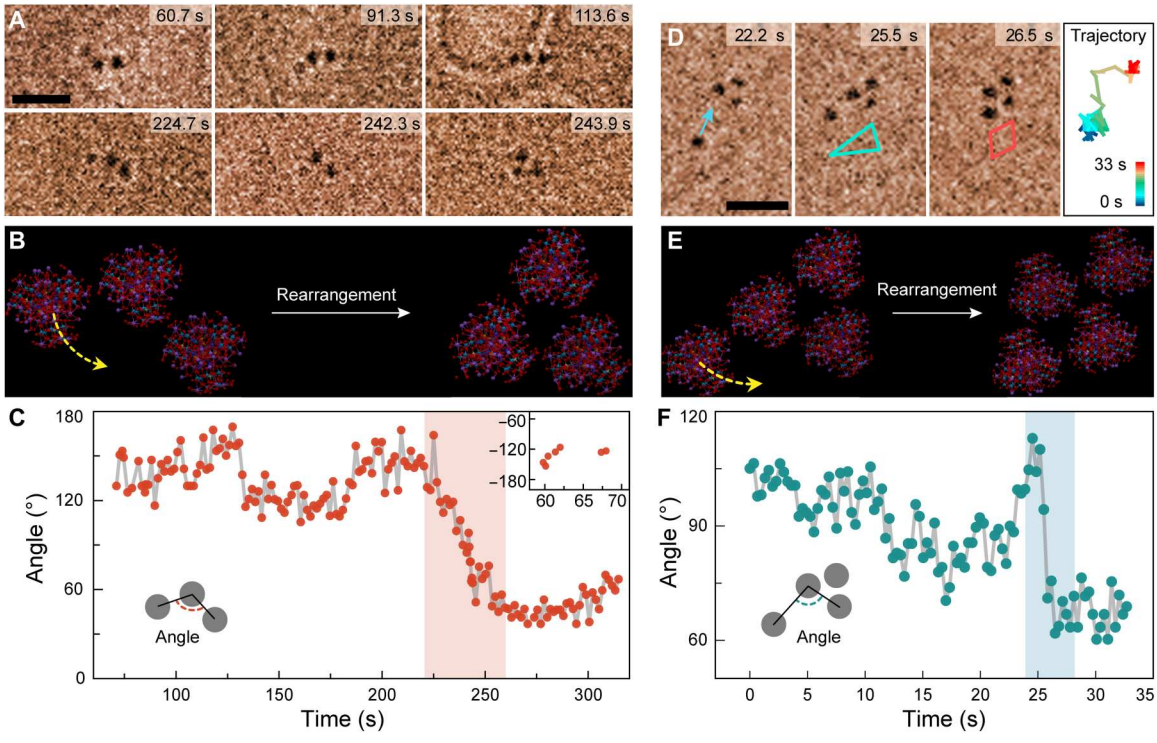

Fig. 5. Formation and pattern rearrangement of CoPOM ion oligomers. (**A** to **C**) Pattern evolution of the trimer. (**D** to **F**) Formation dynamics of the tetramer. (A) Time-series false-color TEM images showing patterns of obtuse triangle (60.7 and 224.7 s), linear shape (93.1 and 113.6 s), and acute triangle (224.7 and 243.9 s). (B) Schematic shows the rearrangement leading to a stable pattern having equilateral triangle configuration. (C) Angle evolution during the observation. The bottom left inset is a sketch illustration of angle calculation. (D) Time-series false-color TEM images showing the formation of a tetramer and trajectory of the additional ion. The insets outline the triangular (25.5 s) and quadrangular (26.5 s) patterns. (E) Schematic shows the pattern rearrangement. (F) Angle evolution. Color-shaded region highlights the process of pattern rearrangement. Scale bars, 10 nm.

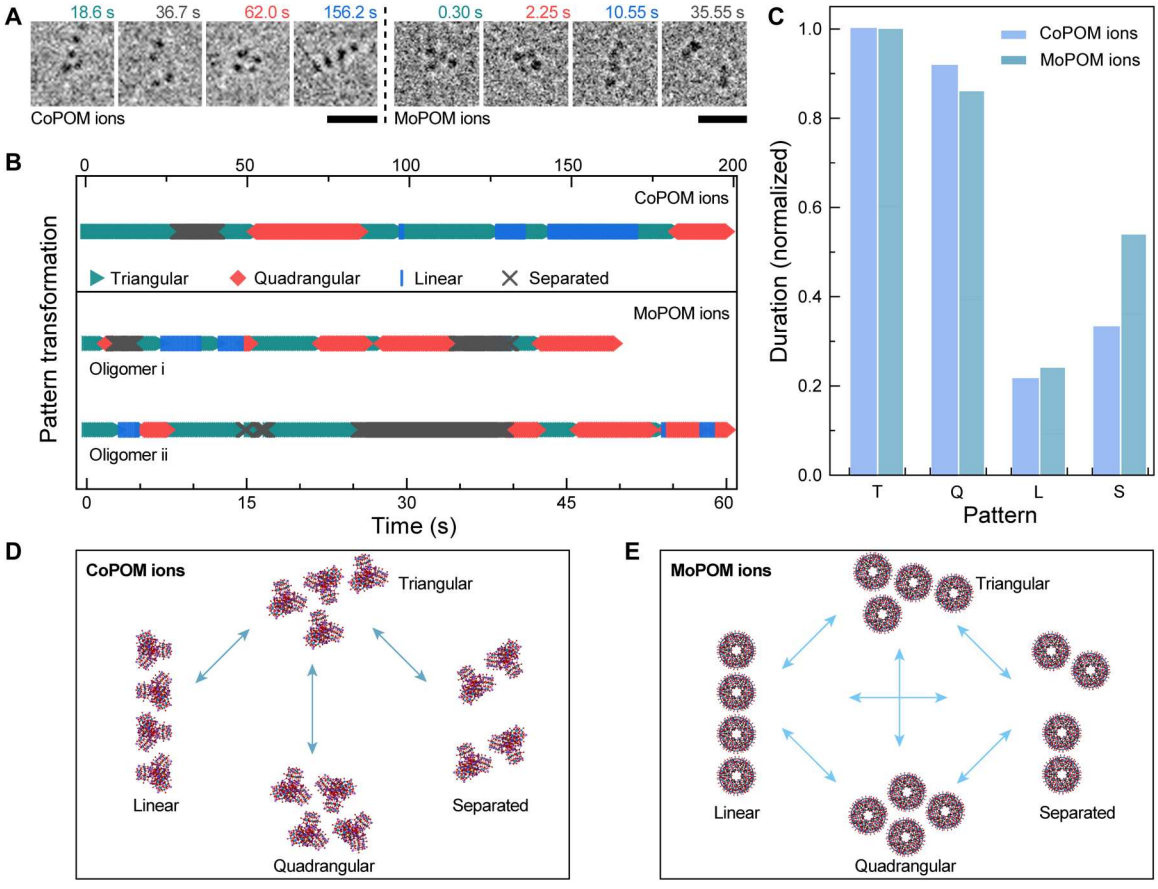

Fig. 6. Dynamic transformation of oligomer pattern. (**A**) Sequential TEM images showing structure transformation between four patterns of tetramers. Left is tetrahedral $[\{Co_4(OH)_3PO_4\}_4(SiW_9O_{34})_4]^{32-}$ (CoPOM) ions (see movie S13), and right is spherical $(NH_4)_{42}[Mo^{VI}_{72}Mo^{V}_{60}O_{372}(CH_3COO)_{30}(H_2O)_{72}]$·ca.300$H_2O$·ca.10$CH_3COONH_4$ (MoPOM) ions (see movie S15). Color code: Cyan, orange, blue, and dark gray indicate triangular (T), quadrangular (Q), linear (L), and separated patterns (S), respectively. Scale bars, 10 nm. (**B**) Pattern evolution of CoPOM oligomers (top; corresponding to movie S13) and MoPOM ions (bottom; corresponding to movies S15 and S16, respectively). (**C**) Normalized duration time of four patterns. (**D** and **E**) Sketch illustrating the pattern transformations. For MoPOM ions, oligomer could transform its configuration between any two of four patterns. For CoPOM ions, only transformations between triangular and three other patterns were observed.

flask at room temperature for 4 days. The precipitated red-brown crystals were filtered; washed with 90% ethanol, pure ethanol, and diethyl ether; and lastly air-dried.

$K_2Na_{30}\{[Co_4(OH)_3PO_4]_4(SiW_9O_{34})_4\}$ (CoPOM) was synthesized according to our previously described method (*43*). Typically, $Na_{10}[\alpha\text{-}SiW_9O_{34}]\cdot 18H_2O$ (1.18 g, 0.40 mmol) was added to a 40 ml of aqueous solution of $CoCl_2\cdot 6H_2O$ (0.78 g, 3.26 mmol). The mixture was stirred until a clear purple solution was obtained. $Na_3PO_4\cdot 12H_2O$ (0.60 g, 1.58 mmol) was then added, and the pH was maintained in the range of 8.5 to 9.0 with 1.0 M KOH (aq). The mixture was stirred for 3 hours at room temperature. After the purple precipitate was removed by filtration, 5 ml of 1.0 M KCl (aq) was added to the obtained filtrate. The solution was stirred for another 30 min and filtered into a 50-ml beaker, followed by slow evaporating at room temperature for 1 week. The precipitated dark purple crystals were collected, then washed with cold water, and air-dried.

In situ liquid phase TEM experiments

About 30 nl of fresh POM solution of 1 mg ml^{-1} was loaded into a nanogap liquid cell with a window of electro-transparent Si_3N_4 membrane (50 μm by 5 μm by 10 nm). There is about 50 nm spacing in between bottom and top chips of the cell. Both chips are pretreated with oxygen plasma to clean the surfaces and render them hydrophilic. Right after the cell sealing, in situ imaging of the POM ions in solution was performed by FEI Cs-corrected Environmental TEM operated at 300 kV, Talos F200S TEM, and Tecnai F20 TEM at 200 kV. Movies were recorded by a complementary metal-oxide semiconductor–based TemCam-XF416 camera (Tietz Video and Image Processing Systems GmbH, Germany) and a Gatan Orius charge-coupled device camera (USA). Electron beam dose rate was controlled in a range from 70 to 90 e $Å^{-2}$ s^{-1}. The dynamics of POM ions in water under high dose rate condition (5940 e $Å^{-2}$ s^{-1}) was presented in fig. S23 and movie S17 and discussed in the Supplementary Materials.

HRTEM simulation

Multislice simulation was conducted to HRTEM images of MoPOM ions acquired in liquid cell. A self-written MATLAB script was used to build the ion models of view directions with a water thickness of 5 nm. HRTEM images were simulated on the basis of the following parameters: accelerating voltage (300 kV),

Cs (5 μm), chromatic aberration coefficient (1 mm), and defocus (80 nm).

Supplementary Materials

This PDF file includes:
Supplementary Text
Table S1
Figs. S1 to S23
Legends for movies S1 to S17
References

Other Supplementary Material for this manuscript includes the following:
Movies S1 to S17

REFERENCES AND NOTES

1. Y. Marcus, in *Ions in Solution and their Solvation* (Wiley, Hoboken, NJ, 2015).
2. G. M. Whitesides, J. P. Mathias, C. T. Seto, Molecular self-assembly and nanochemistry: A chemical strategy for the synthesis of nanostructures. *Science* **254**, 1312–1319 (1991).
3. O. Nordness, J. F. Brennecke, Ion dissociation in ionic liquids and ionic liquid solutions. *Chem. Rev.* **120**, 12873–12902 (2020).
4. Y. Marcus, G. Hefter, Ion pairing. *Chem. Rev.* **106**, 4585–4621 (2006).
5. J. Israelachvili, R. Pashley, The hydrophobic interaction is long range, decaying exponentially with distance. *Nature* **300**, 341–342 (1982).
6. A. A. Verhoeff, M. L. Kistler, A. Bhatt, J. Pigga, J. Groenewold, M. Klokkenburg, S. Veen, S. Roy, T. Liu, W. K. Kegel, Charge regulation as a stabilization mechanism for shell-like assemblies of polyoxometalates. *Phys. Rev. Lett.* **99**, 066104 (2007).
7. T. Fukui, T. Uchihashi, N. Sasaki, H. Watanabe, M. Takeuchi, K. Sugiyasu, Direct observation and manipulation of supramolecular polymerization by high-speed atomic force microscopy. *Angew. Chem. Int. Ed.* **57**, 15465–15470 (2018).
8. P. Tan, N. Xu, L. Xu, Visualizing kinetic pathways of homogeneous nucleation in colloidal crystallization. *Nat. Phys.* **10**, 73–79 (2013).
9. S. F. Tan, S. W. Chee, G. Lin, U. Mirsaidov, Direct observation of interactions between nanoparticles and nanoparticle self-assembly in solution. *Acc. Chem. Res.* **50**, 1303–1312 (2017).
10. H. Hwang, D. A. Weitz, F. Spaepen, Direct observation of crystallization and melting with colloids. *Proc. Natl. Acad. Sci. U.S.A.* **116**, 1180–1184 (2019).
11. U. Gasser, E. R. Weeks, A. Schofield, P. N. Pusey, D. A. Weitz, Real-space imaging of nucleation and growth in colloidal crystallization. *Science* **292**, 258–262 (2001).
12. U. Mirsaidov, J. P. Patterson, H. Zheng, Liquid phase transmission electron microscopy for imaging of nanoscale processes in solution. *MRS Bull.* **45**, 704–712 (2020).
13. J. J. De Yoreo, S. N. A. J. M, Investigating materials formation with liquid-phase and cryogenic TEM. *Nat. Rev. Mater.* **1**, 16035 (2016).
14. J. J. De Yoreo, P. U. Gilbert, N. A. Sommerdijk, R. L. Penn, S. Whitelam, D. Joester, H. Zhang, J. D. Rimer, A. Navrotsky, J. F. Banfield, A. F. Wallace, F. M. Michel, F. C. Meldrum, H. Colfen, P. M. Dove, Crystallization by particle attachment in synthetic, biogenic, and geologic environments. *Science* **349**, aaa6760 (2015).
15. H. G. Liao, D. Zherebetskyy, H. Xin, C. Czarnik, P. Ercius, H. Elmlund, M. Pan, L. W. Wang, H. Zheng, Facet development during platinum nanocube growth. *Science* **345**, 916–919 (2014).
16. N. D. Loh, S. Sen, M. Bosman, S. F. Tan, J. Zhong, C. A. Nijhuis, P. Kral, P. Matsudaira, U. Mirsaidov, Multistep nucleation of nanocrystals in aqueous solution. *Nat. Chem.* **9**, 77–82 (2017).
17. J. Baumgartner, A. Dey, P. H. Bomans, C. Le Coadou, P. Fratzl, N. A. Sommerdijk, D. Faivre, Nucleation and growth of magnetite from solution. *Nat. Mater.* **12**, 310–314 (2013).
18. M. W. van de Put, C. C. Carcouet, P. H. Bomans, H. Friedrich, N. de Jonge, N. A. Sommerdijk, Writing silica structures in liquid with scanning transmission electron microscopy. *Small* **11**, 585–590 (2015).
19. H. Zheng, Imaging, understanding, and control of nanoscale materials transformations. *MRS Bull.* **46**, 443–450 (2021).
20. N. Clark, D. J. Kelly, M. Zhou, Y.-C. Zou, C. W. Myung, D. G. Hopkinson, C. Schran, A. Michaelides, R. Gorbachev, S. J. Haigh, Tracking single adatoms in liquid in a transmission electron microscope. *Nature* **609**, 942–947 (2022).
21. P. Yin, D. Li, T. Liu, Solution behaviors and self-assembly of polyoxometalates as models of macroions and amphiphilic polyoxometalate-organic hybrids as novel surfactants. *Chem. Soc. Rev.* **41**, 7368–7383 (2012).
22. Y. Gao, S. A. Eghtesadi, T. Liu, Supramolecular structures formation of polyoxometalates in solution driven by counterion–macroion interaction, in *Advances in Inorganic Chemistry* (Elsevier, 2017), vol. 69, chap. 2, pp. 29–65.
23. M. Hutin, M. H. Rosnes, D. L. Long, L. Cronin, Polyoxometalates: synthesis and structure – From building blocks to emergent materials, in *Comprehensive Inorganic Chemistry II*, J. Reedijk, K. Poeppelmeier, Eds. (Elsevier, ed. 2, 2013), vol. 2, pp. 241–269.
24. T. Liu, Hydrophilic macroionic solutions: What happens when soluble ions reach the size of nanometer scale? *Langmuir* **26**, 9202–9213 (2010).
25. R. E. Schreiber, L. Houben, S. G. Wolf, G. Leitus, Z. L. Lang, J. J. Carbo, J. M. Poblet, R. Neumann, Real-time molecular scale observation of crystal formation. *Nat. Chem.* **9**, 369–373 (2017).
26. J. A. Soltis, C. M. Wallace, R. L. Penn, P. C. Burns, Cation-dependent hierarchical assembly of U_{60} nanoclusters into macro-ion assemblies imaged via cryogenic transmission electron microscopy. *J. Am. Chem. Soc.* **138**, 191–198 (2016).
27. S. Mogurampelly, J. R. Keith, V. Ganesan, Mechanisms underlying ion transport in polymerized ionic liquids. *J. Am. Chem. Soc.* **139**, 9511–9514 (2017).
28. H. Liu, X. Luo, A. P. Sokolov, S. J. Paddison, Quantitative evidence of mobile ion hopping in polymerized ionic liquids. *J. Phys. Chem. B* **125**, 372–381 (2021).
29. K. Dokko, D. Watanabe, Y. Ugata, M. L. Thomas, S. Tsuzuki, W. Shinoda, K. Hashimoto, K. Ueno, Y. Umebayashi, M. Watanabe, Direct evidence for Li ion hopping conduction in highly concentrated sulfolane-based liquid electrolytes. *J. Phys. Chem. B* **122**, 10736–10745 (2018).
30. J. H. Choi, H. Lee, H. R. Choi, M. Cho, Graph theory and ion and molecular aggregation in aqueous solutions. *Annu. Rev. Phys. Chem.* **69**, 125–149 (2018).
31. C. Huang, K. T. Wikfeldt, T. Tokushima, D. Nordlund, Y. Harada, U. Bergmann, M. Niebuhr, T. M. Weiss, Y. Horikawa, M. Leetmaa, M. P. Ljungberg, O. Takahashi, A. Lenz, L. Ojamae, A. P. Lyubartsev, S. Shin, L. G. Pettersson, A. Nilsson, The inhomogeneous structure of water at ambient conditions. *Proc. Natl. Acad. Sci. U.S.A.* **106**, 15214–15218 (2009).
32. U. Anand, J. Lu, D. Loh, Z. Aabdin, U. Mirsaidov, Hydration layer-mediated pairwise interaction of nanoparticles. *Nano Lett.* **16**, 786–790 (2016).
33. H. G. Liao, L. Cui, S. Whitelam, H. Zheng, Real-time imaging of Pt_3Fe nanorod growth in solution. *Science* **336**, 1011–1014 (2012).
34. E. Allahyarov, I. D'Amico, H. Löwen, Attraction between like-charged macroions by coulomb depletion. *Phys. Rev. Lett.* **81**, 1334–1337 (1998).
35. Z. Liu, T. Liu, M. Tsige, Elucidating the origin of the attractive force among hydrophilic macroions. *Sci. Rep.* **6**, 26595 (2016).
36. J. Chen, M. K. Bera, H. Li, Y. Yang, X. Sun, J. Luo, J. Baughman, C. Liu, X. Yao, S. S. C. Chuang, T. Liu, Accurate determination of the quantity and spatial distribution of counterions around a spherical macroion. *Angew. Chem. Int. Ed.* **60**, 5833–5837 (2021).
37. J. M. Pigga, M. L. Kistler, C. Y. Shew, M. R. Antonio, T. Liu, Counterion distribution around hydrophilic molecular macroanions: The source of the attractive force in self-assembly. *Angew. Chem. Int. Ed.* **48**, 6538–6542 (2009).
38. A. Chaumont, G. Wipff, Interactions between keggin anions in water: The higher their charge, the higher their condensation? A simulation study. *Eur. J. Inorg. Chem.* **2013**, 1835–1853 (2013).
39. J. N. Israelachvili, in *Intermolecular and Surface Forces* (Academic Press, San Diego, CA, ed. 3, 2011).
40. A. Chaumont, G. Wipff, Ion aggregation in concentrated aqueous and methanol solutions of polyoxometallates Keggin anions: The effect of counterions investigated by molecular dynamics simulations. *Phys. Chem. Chem. Phys.* **10**, 6940–6953 (2008).
41. A. Chaumont, G. Wipff, Do Keggin anions repulse each other in solution? The effect of solvent, counterions and ion representation investigated by free energy (PMF) simulations. *C. R. Chim.* **15**, 107–117 (2012).
42. J. Z. Wu, D. Bratko, H. W. Blanch, J. M. Prausnitz, Monte Carlo simulation for the potential of mean force between ionic colloids in solutions of asymmetric salts. *J. Chem. Phys.* **111**, 7084–7094 (1999).
43. X. B. Han, Z. M. Zhang, T. Zhang, Y. G. Li, W. Lin, W. You, Z. M. Su, E. B. Wang, Polyoxometalate-based cobalt-phosphate molecular catalysts for visible light-driven water oxidation. *J. Am. Chem. Soc.* **136**, 5359–5366 (2014).
44. X. Lopez, C. Bo, J. M. Poblet, Electronic properties of polyoxometalates: Electron and proton affinity of mixed-addenda Keggin and Wells-Dawson anions. *J. Am. Chem. Soc.* **124**, 12574–12582 (2002).
45. F. Leroy, P. Miro, J. M. Poblet, C. Bo, J. Bonet Avalos, Keggin polyoxoanions in aqueous solution: Ion pairing and its effect on dynamic properties by molecular dynamics simulations. *J. Phys. Chem. B* **112**, 8591–8599 (2008).

46. A. Müller, E. Krickemeyer, H. Bögge, M. Schmidtmann, F. Peters, Organizational forms of matter: An inorganic super fullerene and keplerate based on molybdenum oxide. *Angew. Chem. Int. Ed.* **37**, 3359–3363 (1998).
47. H. G. Liao, H. Zheng, Liquid cell transmission electron microscopy. *Annu. Rev. Phys. Chem.* **67**, 719–747 (2016).
48. P. Ercius, J. A. Hachtel, R. F. Klie, Chemical and bonding analysis of liquids using liquid cell electron microscopy. *MRS Bull.* **45**, 761–768 (2020).
49. M. N. Yesibolati, S. Laganá, S. Kadkhodazadeh, E. K. Mikkelsen, H. Sun, T. Kasama, O. Hansen, N. J. Zaluzec, K. Mølhave, Electron inelastic mean free path in water. *Nanoscale* **12**, 20649–20657 (2020).
50. S. M. Seltzer, M. J. Berger, Evaluation of the collision stopping power of elements and compounds for electrons and positrons. *Int. J. Appl. Radiat. Isot.* **33**, 1189–1218 (1982).
51. N. M. Schneider, M. M. Norton, B. J. Mendel, J. M. Grogan, F. M. Ross, H. H. Bau, Electron–water interactions and implications for liquid cell electron microscopy. *J. Phys. Chem. C* **118**, 22373–22382 (2014).
52. H. Zheng, R. K. Smith, Y.-W. Jun, C. Kisielowski, U. Dahmen, A. P. Alivisatos, Observation of single colloidal platinum nanocrystal growth trajectories. *Science* **324**, 1309–1312 (2009).
53. Y. Liu, X.-M. Lin, Y. Sun, T. Rajh, In situ visualization of self-assembly of charged gold nanoparticles. *J. Am. Chem. Soc.* **135**, 3764–3767 (2013).
54. U. M. Mirsaidov, H. Zheng, D. Bhattacharya, Y. Casana, P. Matsudaira, Direct observation of stick-slip movements of water nanodroplets induced by an electron beam. *Proc. Natl. Acad. Sci. U.S.A.* **109**, 7187–7190 (2012).
55. H. Zheng, S. A. Claridge, A. M. Minor, A. P. Alivisatos, U. Dahmen, Nanocrystal diffusion in a liquid thin film observed by in situ transmission electron microscopy. *Nano Lett.* **9**, 2460–2465 (2009).
56. S. W. Chee, Z. Baraissov, N. D. Loh, P. T. Matsudaira, U. Mirsaidov, Desorption-mediated motion of nanoparticles at the liquid–solid interface. *J. Phys. Chem. C* **120**, 20462–20470 (2016).
57. V. Jamali, C. Hargus, A. Ben-Moshe, A. Aghazadeh, H. D. Ha, K. K. Mandadapu, A. P. Alivisatos, Anomalous nanoparticle surface diffusion in LCTEM is revealed by deep learning-assisted analysis. *Proc. Natl. Acad. Sci. U.S.A.* **118**, e2017616118 (2021).
58. S. W. Chee, U. Anand, G. Bisht, S. F. Tan, U. Mirsaidov, Direct observations of the rotation and translation of anisotropic nanoparticles adsorbed at a liquid–solid Interface. *Nano Lett.* **19**, 2871–2878 (2019).

Acknowledgments

Funding: This work was supported by the National Natural Science Foundation of China (grants no. 22288102, U22A20396, 3210127, 22021001, 21673198, 21991151, 21991150, and 91934303), by the Fundamental Research Funds for the Central Universities (20720220009), and by the National Key Research and Development Program of China grant no. 2017YFA0206500. This work was also supported by the U.S. Department of Energy, Office of Science, Office of Basic Energy Sciences (BES), Materials Sciences and Engineering Division under contract no. DE-AC02-05-CH11231 within the in situ TEM program (KC22ZH). **Author contributions:** Conceptualization: S.L., X.H., and H.-G.L. Methodology: S.L., X.H., Y.-Z.T., S.-G.S., H.Z., and H.-G.L. Investigation: S.L., X.H., C.O., Y.-H.J., Y.S., T.Z., F.Y., and M.G. Visualization: S.L., C.O., and S.Z. Funding acquisition: H.-G.L. Project administration: H.Z. and H.-G.L. Supervision: H.Z. and H.-G.L. Writing (original draft): S.L. Writing (review and editing): S.L., X.H., H.Z., and H.-G.L. **Competing interests:** The authors declare that they have no competing interests. **Data and materials availability:** All data needed to evaluate the conclusions in the paper are present in the paper and/or the Supplementary Materials. The crystallographic information files of MoPOM and CoPOM ionic structures (CSD numbers 410097 and 426579, respectively) were obtained from the FIZ Karlsruhe Inorganic Crystal Structure Database (ICSD; http://fiz-karlsruhe.de/icsd.html).

Submitted 20 November 2022
Accepted 26 June 2023
Published 28 July 2023
10.1126/sciadv.adf8436